J. Braz. Chem. Soc., Vol. 7, No. 3, 199-208, 1996.
Printed in Brazil.

0103 – 5053 $6.00 + 0.00

Article

Some Aspects of X-Ray Absorption Spectroscopy: The Interplay Between Models and Experiments

Agnès Traverse

LURE, UMR 130-CNRS, Bâtiment 209A, 91405 Orsay campus, France

Received: January 26, 1996

A espectroscopia de absorção de raios X (EAX) é apresentada principalmente por meio de exemplos selecionados, como uma técnica que permite sondar ambientes atômicos e eletrônicos que circunvizinham um dado tipo de átomo. Após breve descrição teórica dos processos atômicos que levam a um espectro de absorção são discutidos alguns exemplos, como os relacionados com o crescimento da estrutura de camadas de óxidos e a evolução da composição química de catalisadores após tratamentos térmicos. Atenção especial é dada às novas disponibilidades de programas computacionais, agora acessíveis, que consideram processos de espalhamento simples e múltiplos e que, em muitos casos, têm auxiliado no entendimento dos resultados experimentais.

X-ray Absorption Spectroscopy (XAS) is mainly presented through some experimental examples as a technique able to locally probe the atomic and electronic environment surrounding a given type of atom. After a very short theoretical description of the atomic processes leading to an absorption spectrum, some examples are discussed, including the structural growth of a oxide layers, and the evolution of the chemical composition of catalysts after thermal treatments. Special attention is given to the capabilities of computer programs now available which take into account single and multiple scattering processes, and in many cases have helped in the understanding of experimental results.

Keywords: *EXAFS, X-ray absorption spectroscopy*

Introduction

X-ray absorption spectroscopy (XAS) permits the investigation of the local environment around a given atom in a matrix in terms of the number of neighbors and distances. The great advantage is that structural information can be obtained for samples with short range order, whereas another technique which also provides structural information, X-ray diffraction, requires long range order. In addition, samples can be studied regardless of their state, whether gas, liquid or solid, or whether metal, semiconductor or insulator.

The basic process, which has been well-described in textbooks[1], is as follows: a photon beam with an intensity, I_0, and a varying incident energy, E, is sent onto a specimen. The intensity recorded behind it, I_1, displays sharp jumps, occurring at specific energies depending, on the nature of the atoms present in the material (Fig. 1). These jumps correspond to the absorption of a photon by a core electron, either s, p or d, leading to a loss of intensity of the incident beam. Typically, the absorption of 1s electron occurs at an energy of 1839 eV in Si, at 7112 eV in Fe, and at 25514 eV in Ag. The fact that the absorption occurs at different energies for different atoms provides the selectivity of the technique. If the energy given to the absorbing electron is a little bit larger than its binding energy, the electron jumps to empty electronic states. The recorded intensity up to some 50 eV above the absorption edge is related to the density of unoccupied states. This energy range is called the X-ray Absorption Near-Edge Structure (XANES). If the transmitted energy is increased, the electron is ejected into the vacuum. This can be represented by an emitted wave which will be backscattered by the neighbors. The interaction between the emitted and the backscattered waves gives rise to interferences whose intensity is related to the nature and number of neighbors, whereas the frequency is correlated to the distance between the emitting atom and the neighbors (Fig. 2). This energy range from 50 to 1000 eV above the absorption edge is called the Extended X-ray Absorption Fine Structure (EXAFS) region.

A quantitative analysis of the oscillations provides the number and distance between neighbors. In this way, the

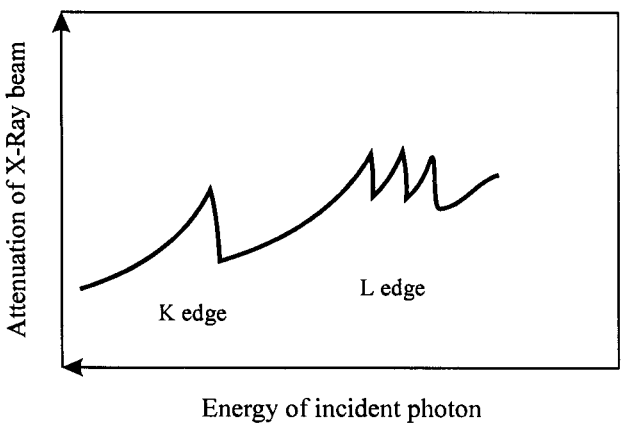

Figure 1. X-ray absorption spectrum showing the K and L edges.

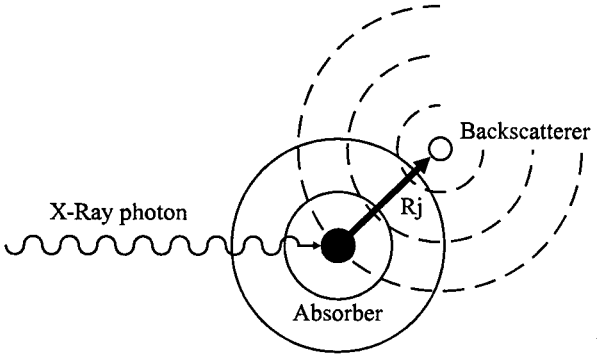

Figure 2. Schematic of the EXAFS process showing the backscattered wave interferring with the emitted one.

first, second and third shells, etc. around a given atom in the sample studied can usually be well characterized.

In the transmission mode described above, the intensity of the transmitted beam is measured, so the specimen has to be thin, typically on the order of a few microns. However both fluorescence emission (more probable for $Z > 30$) and secondary electron emission (more probable for $Z < 30$) take place from the surface of the specimen. They result from the de-excitation of the absorber (Fig. 3), and are correlated to the photon absorption. The escape depth for electrons is on the order of 100 to 1000 Å, depending on the energy absorption and on a few microns for the fluorescence photons. Thus a sample too thick to be investigated in the transmission mode can be analyzed either in the fluorescence mode or in the total electron yield (TEY) mode. The TEY mode offers the advantage of making it possible to study the evolution of the sample surface (the surface meaning a thickness as defined above) submitted to external modifications, such as chemical or mechanical perturbations. Nevertheless, a limitation can come from the concentration of the absorber in the matrix. Typically, in the transmission or TEY detection modes, concentrations of a few atomic percent are required (*i.e.* about 10^{16} at.cm^{-2}),

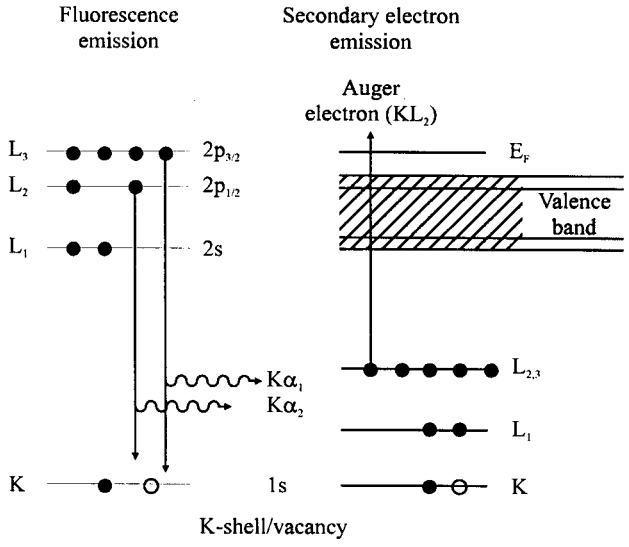

Figure 3. De-excitation via fluorescence or electron emission.

whereas in the fluorescence mode concentrations 10 and even 100 times lower can be achieved.

XAS thus appears to be a very versatile technique for obtaining information on short range order, specifically around one type of atom in the specimen. The high flux emitted in synchrotron rings has allowed a great development of the technique. Several review papers have already been published on XAS spectroscopy[2,3]. Using some examples in this paper will be limited to some information provided through the XAS technique, the complementary aspects of XANES and EXAFS features, and the possible interplay between calculated and experimental spectra.

In the next section, the principle of XAS is briefly presented, together with the different models which account for the observed signal. Several computer programs are mentioned which perform calculations of the XAS spectra, followed by some indications for experimental details and the data treatment of the EXAFS oscillations. The last section is devoted to examples.

X-ray absorption spectroscopy

Principle

The X-ray absorption coefficient, $\mu_i(E)$, due to the excitation of an electron from a core level, i, to an empty state, f, is described in the dipole approximation by (1):

$$\mu_i(E) = \frac{4\pi^2}{\Omega} \alpha E \sum_f | < \psi_i | \hat{e} . r | \psi_f >^2 \delta (E - E_f + E_i) | \quad (1)$$

where E_i and E_f are the energies of the initial and final states, Ω is the unit cell volume, $\alpha = 2\pi e^2/hc$, $\hat{e}$ is the polarization vector of the incident photon, and r is the vector between the absorber and the backscatterer. The initial state is described by the wave function ψ_i. The

problem is to evaluate the wave function corresponding to the final states ψ_f. In the energy range from 50 eV up to 1000 eV above the edge, where the mean free path of the ejected electron is short, a single scattering approach is valid in principle, thus ψ_f is the wave function due to single backscattering by the neighboring atoms. At low energies, up to 50 eV above the absorption edge, where the mean free path of the ejected electron is large, both transitions of the ejected electrons to unoccupied electronic levels and multiple scattering effects have to be taken into account (Fig. 4). The fact that the photon beam is polarized, which gives rise to the scalar product, could play a role when r vectors with specific directions are present in the analyzed samples, in the case of single crystals for example.

Single scattering approach

Here we consider that the electronic mean free path is such that only one scattering process between the central atom and a neighboring one takes place, or that only two atoms are involved. In the dipole approximation, taking into account two correction terms, namely i) inelastic effects due to lattice vibrations (hence correlated to the sample temperature), and ii) inelastic losses inducing a modification of the wave vector k, the expression of the oscillations is given by (1):

$$k\chi(k) = \sum_j \frac{N_j}{r_j^2} |f_j(k,\pi)| \sin[2kr_j + \phi_j(k)] e^{-2\sigma_j^2 k^2} e^{-2r_j/\lambda_j(k)}$$

The wave vector is deduced from the energy E, given in eV by:

$$k[\text{Å}^{-1}] = [(\frac{8\pi^2 m}{h^2})(E - E_0)]^2 = 0.5123(E - E_0)^{1/2}$$

where f is the probability of backscattering at 180° by the atom j located on shell j at distance r_j from the absorber.

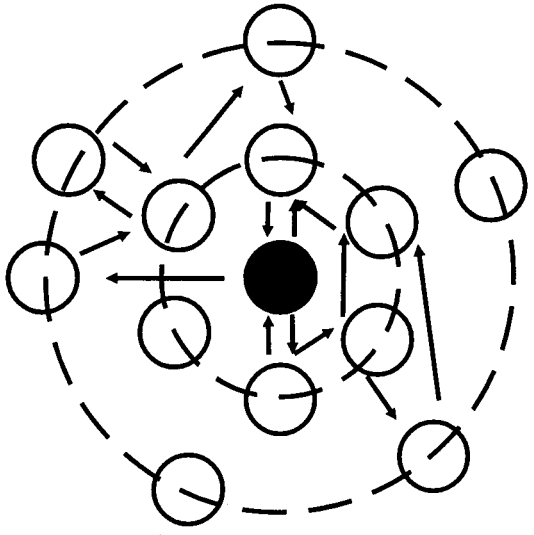

Figure 4. Scheme of the multiscattering process.

There are N_j neighbors in this shell, and ϕ_j is the phase shift. The first correction term contains the Debye-Waller factor σ_j, which is a measure of the structural and thermal disorders. The second correction term contains the mean free path of the photoelectrons, λ_j.

These oscillations must be extracted from the absorption spectrum $\mu(E)$. The steps are: i) substraction of a pre-absorption background due to other absorption processes occuring in the target, and ii) substraction of the atomic absorption term, μ_0, the one observed if the absorbers are not surrounded by other atoms. Then $\chi(E)$ is written:

$$\chi(E) = \frac{(\mu - \mu_0)}{\mu_0}$$

The experimental spectrum is then converted in a k scale and a Fourier transform is calculated in order to obtain the peaks corresponding to the positions r_j of the neighboring shells. The Fourier transform can be seen as a pseudoradial function (PRF). An example of an absorption spectrum, an EXAFS spectrum and its corresponding Fourier transform is given in Fig. 5 for the case of Cu.

To obtain quantitative information on the local environment, *i.e.* the number of neighbors in a given shell and its distance from the absorbing atom, the peak of interest is selected and an inverse Fourier transform is calculated. By a fitting procedure, if f and ϕ are known for this specific absorber-backscatterer combination, N and r can be deduced. Several software packages, running on either PC or Macintosh, have been written to perform these data treatments[4].

One problem is to know the f and ϕ quantities. They can either be deduced either from well-known standard samples or taken from the tables in McKale[5] or Teo and Lee[6], for example.

In fact, the single scattering model has limitations. For large electronic paths, the distance experienced in a single scattering process might be very similar to a distance made by multiple scattering on several shells. For example, in Cu the distance of 4.42 Å corresponding to the third shell is very close to the distance of 4.36 Å due to two scatterings on the first shell. Hence, the treatment of the first and second shell remains valid in the single scattering model, but the treatment of shells at larger distances is probably less reliable.

Multiple scattering approach - band structure approach

The absorption process is now examined in the low energy range where excited electrons fill empty states and experience multiple scattering (MS) on the neighboring atoms with scattering angles differing from 180°. An interpretation of the XANES features can thus be done either in the electronic band structure approach or in the MS one. The two approaches are equivalent in principle, as demon-

strated by Müller[7]. The disadvantage of an electronic band structure approach is that a periodic potential is required to perform such calculations, which is not the case in all the systems studied. Moreover these calculations are often time-consuming. Hence, in several cases, and especially for amorphous systems, an MS approach is the only suitable one. Several computer programs, such as FEFF[8], CONTINUUM[9], GNXAS[10] have made such calculations possible.

Because the electron sees several different atomic sites, this part of the spectrum is extremely sensitive to the chemical environment of the probed atom[11]. By comparing spectra recorded from several samples with known and unknown surroundings, it is sometimes possible to interpret the observed features and to deduce the local order around the probed atom.

An example is given in Fig. 6 where the Ti K edge XANES for the two structural states of titanium oxide, anatase and rutile[12], are plotted. The shape of the near-edge spectrum is a good fingerprint for determining the type of Ti oxide which grows. Rutile and anatase have different Ti local environments. In both cases, a Ti atom is surrounded by 6 O. But the octahedra are not deformed in the same

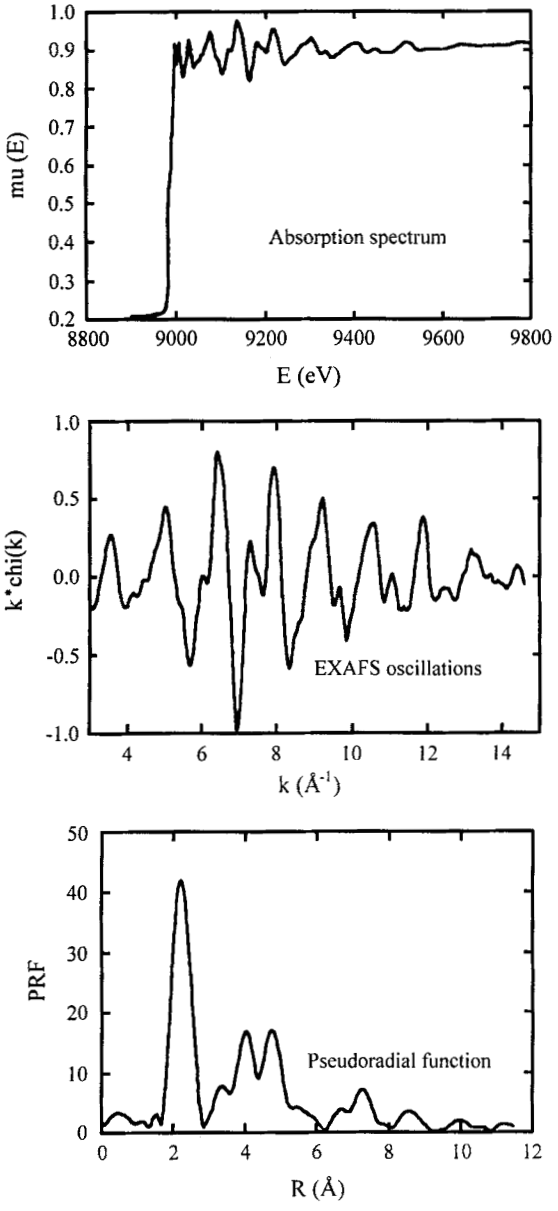

Figure 5. An example of an absorption spectrum, its corresponding EXAFS oscillations and PRF: the case of Cu.

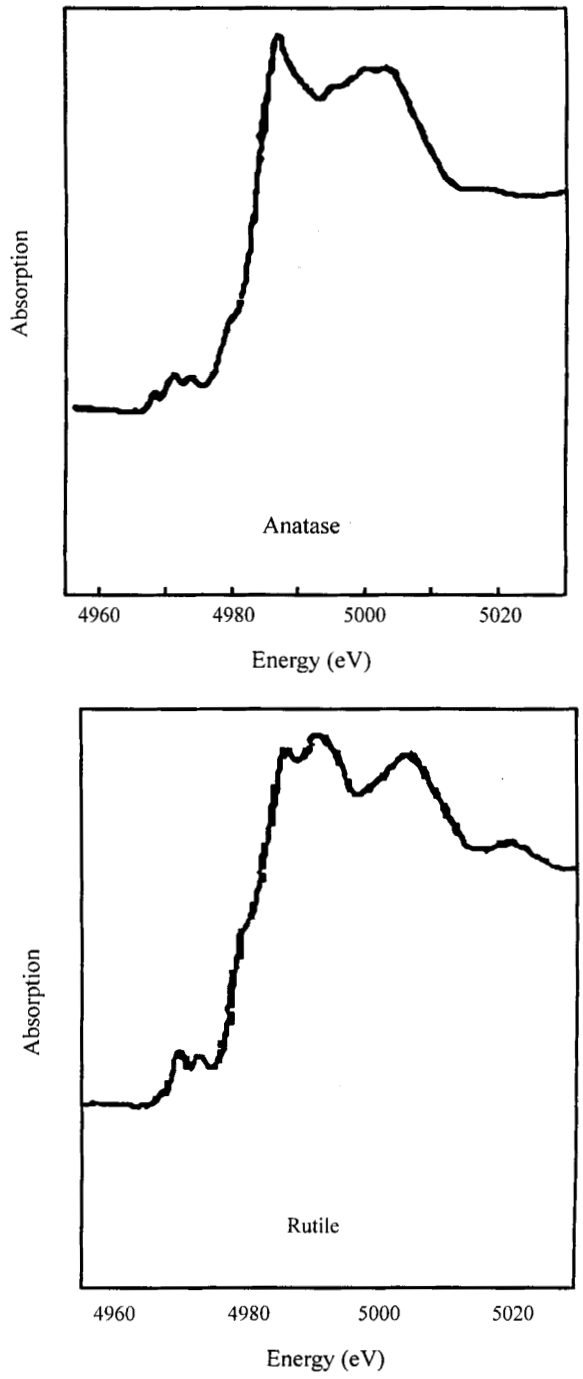

Figure 6. Ti K edge XANES in anatase (a) and rutile (b).

way. In rutile, there are 4 O at 1.946 Å and 2 at 1.984 Å, and the symmetry group is D_{2h}. In anatase, the corresponding distances are 1.937 Å and 1.964 Å, and the symmetry group is D_{2d}. The difference in the group symmetry is clearly evidenced in the XANES shapes.

Experimental conditions

In XAS experiments, a standard measurement consists of measuring i) the number of photons incident on the sample, and ii) the number of photons transmitted by the sample if working in the transmission mode, or the number of electrons or photons emitted if working in the TEY or fluorescence modes, respectively. The photon or electron yield is recorded while the monochromator scans the energy of the incident photon beam from E_1 (about 80 eV below the absorption edge E_0) to E_2 (about 1000 eV above E_0). Specific detectors have been developed to optimize the quality of the experimental data. The dispersive mode is an example of this optimization[13].

The samples must display an optimum thickness in the transmission mode, typically 5 μm for Ti, and 25 μm for Ag, the rules being that the best signal to noise ratio is given by $\Delta\mu = 1$ at the edge[1]. For thicker specimens, TEY and fluorescence modes are used. The probed depth in the TEY mode has been studied, in Refs. 14 and 15 for example. In the case of disordered systems where the EXAFS oscillations are weakened, a low temperature measurement (80 K) is useful in the data treatment because of a decrease of the Debye Waller factor[16].

Experimental fators can modify the parameters supposed to describe a local environment, such as insufficient energy resolution of the monochromator, which induces a smearing of the oscillations, contamination of the incident radiation by harmonics, X-ray leakage around the sample holder, and sample heterogeneity. All these problems are discussed in Ref. 17.

Some Experimental Examples

Nitrides: a band structure approach to XANES

An example is presented with the study of TiN_x and VN_x with x varying from 1 to 0.53 and 1 to 0.72, respectively[18]. The band structures of these compounds were calculated using the Korringa-Kohn-Rostoker coherent potential approximation (KKR-CPA) which considers a disordered metal non-metal vacancy system[19]. The Ti and V K edge XANES spectra recorded for TiN_x and VN_x (Fig. 7) display a peak intensity at 20 eV from the onset. This peak represents the a_{1g} (s*) and t_{1u} (s*, p*) anti-bonding orbitals with a respective 4s and 4p character, mixed with N 2p orbitals. In the energy range from 0 to 11 eV the evolution with x is different in TiN_x and VN_x. The KKR-CPA calculations offer an interpretation of this behavior: this energy range is attributed to vacancy states. The calculation predicts that in TiN_x, (i) empty vacancy states will appear for $x < 0.6$ and (ii) these states move from below to above the Fermi level.

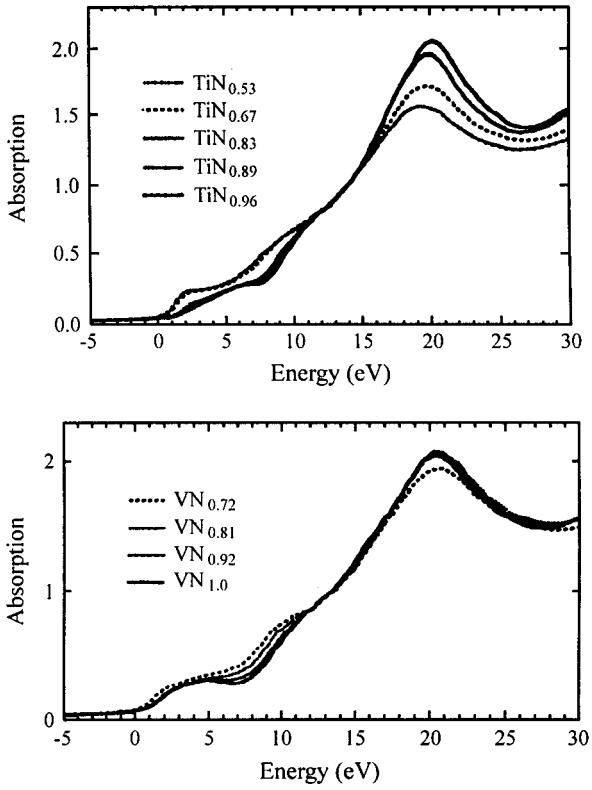

Figure 7. Ti and V K edge XANES recorded from TiN_x (a) and VN_x (b) (from Ref. 18).

This is in good agreement with the observed variation, where for x = 0.96, 0.89, and 0.83 the structure intensity remains the same, while it increases for x = 0.67 and 0.53. In VN_x, the same calculation predicts that the Fermi level lies above the vacancy states, whatever the vacancy concentration. Again, this is in good agreement with the absence of strong modifications in VN_x. The metal 4p states are hybridized with non-metal p states, and are therefore particularly sensitive to vacancies at the N sites. This is in line with previous observations of occupied electronic densities of states[20].

Cu clusters: a multiple scattering approach to XANES

Ion implantation is a good tool for introducing impurities into a target at a depth on the order of 100 to 1000 Å. When the impurities are insoluble in the matrix, they form precipitates whose size can be monitored by the implantation fluency[21]. XAS is particularly useful for detecting these precipitates, especially when they are too small to be easily seen by either transmission electron microscopy or X-ray diffraction. Here an example of Cu implantion in AlN bulk ceramic is presented. The Cu ion energy was on the order of 100 keV, leading to a profile located at a depth

of about 500 Å. The fluencie were varied from 5 x 10^{16} at.cm^{-2} to 5 x 10^{17} at.cm^{-2} to reach different Cu concentrations. Some samples were annealed at 800 °C for 1 h, and measured by XAS at the Cu K edge. Typical PRF obtained from EXAFS oscillations recorded in the TEY mode are shown in Fig. 8, together with the one for pure Cu.

It is clear that the local environment of implanted Cu is rather close to the one of pure Cu, and that the fcc crystalline arrangement is kept. The difference in the intensity of the PRF comes from the fact that around a given Cu there are fewer atoms than in pure Cu. The only possible explanation is that clusters are formed with varying diameters. In clusters, the atoms on the outside have fewer neighbors than at the center, leading to a smaller average number of neighbors. Diameters varying from 5 to 20 Å are deduced. The XANES spectra are shown in Fig. 9 for pure Cu, and for clusters with 20 Å and 9 Å in diameter. For pure Cu, a two peak structure is seen which corresponds to the p electronic empty states. For the smaller clusters there is a modification of the two peak structure, the second being smeared out. FEFF calculations[8], based on a multiscattering approach, performed on both a large and a small Cu cluster, reproduce very well the experimental behavior (Fig. 9). This is for a diameter smaller than 10 Å that the empty p state distribution is modified in agreement with the experimental results[22]. A calculation of the electronic states in clusters by Messmer *et al.*[23] qualitatively leads to the same conclusion: for small clusters, there are fewer electronic states above the Fermi level.

Co based catalysts: interplay between XANES and EXAFS

In Ref. 24, the authors try to understand the activity of two catalysts *versus* temperature. Cobalt phthalocyanine and the polyacrylonitrile + cobalt acetate display a maximum electrocatalytic activity for O_2 reduction at 850 °C and 950 °C, respectively. As this maximum might be related to a change in the structural arrangement, they performed XAS from 300 °C up 1000 °C. Measurements

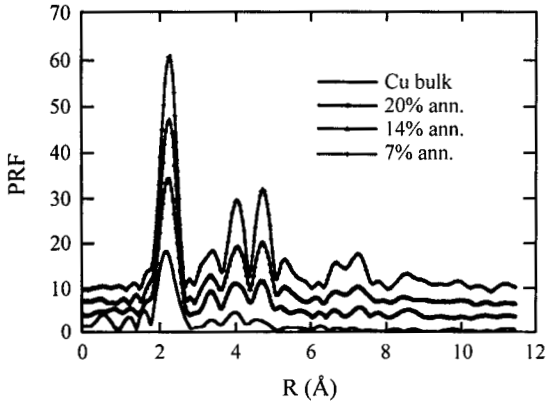

Figure 8. PRF of a Cu foil as compared to PRF of Cu clusters prepared by Cu implantation in an AlN matrix.

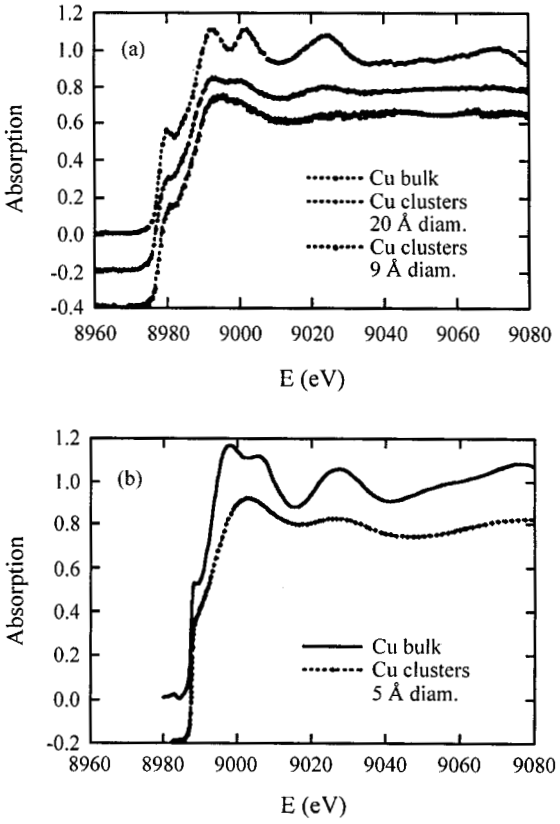

Figure 9. Cu K edge XANES for a pure Cu foil and for Cu clusters with a 20 Å and 9 Å diameter (a). FEFF calculations for a Cu foil and a Cu cluster with a 5 Å diameter (b).

were done at the Co K edge in the transmission mode, and at the N K edge in the TEY mode. The evolution of the XANES spectra and PRF extracted from the EXAFS oscillations for the cobalt phthalocyanine is shown on Fig. 10. There is an evolution from a Co-N_4 center (Co site surrounded by 4 N atoms) to a Co site surrounded by Co atoms. The formation of Co clusters takes place during annealing and the maximum activity is clearly related to a cluster diameter of 20 Å. From the XANES spectra taken at the N edge, it appears that N is no longer detected above 900 °C, which corroborates the change in the Co surroundings previously mentioned.

The initial environment of Co of the Co-N_4 type is unequivocally identifed by the feature located at 8 eV in the XANES and this feature disappears so that the XANES of metallic Co is observed. There is no intermediate step via an oxide structure as is sometimes suggested for this type of catalytic reaction[25]. The authors emphasized the fact that EXAFS data are difficult to interpret, especially when light elements like O or N are surrounding the probed atom, because the amplitude factors and phase shifts are too close for both neighbors to be able to distinguish them via the PRF only. This is the reason that the XANES and EXAFS measurements were carried out simultaneously.

Titanium anodic oxidation: a short range order characterization

Thin oxide layers were obtained by the electrochemical oxidation of bulk Ti[26]. In the precursor state, that is for thicknesses ranging from 150 to 1050 Å, the layers appeared to be amorphous. So, neither the type of grown Ti oxide (anatase or rutile) nor the growth mode could be studied. It is only after aging under electrical polarization or thermal treatment that grazing X-ray diffraction could be performed, revealing the appearance of crystallization in the anatase form. XAS was performed at the Ti edge using the TEY mode in order to study the sample depth concerned by the oxidation process. The amorphous layers grow with a short range order similar to that of anatase, as seen in Fig. 11, where the spectrum recorded on a 500 Å thick amorphous layer is plotted together with that of anatase. The quantitative analysis of the EXAFS data revealed that short range order is present in the 3 Å range around Ti, with a first O shell and a second Ti shell, corresponding to small aggregates of 11 atoms. The lattice distances in these clusters are somewhat smaller than in the crystal, indicating a compaction effect induced by the metal oxide boundary. During crystallization, the growth occurs in platelets in agreement with previous observations[27].

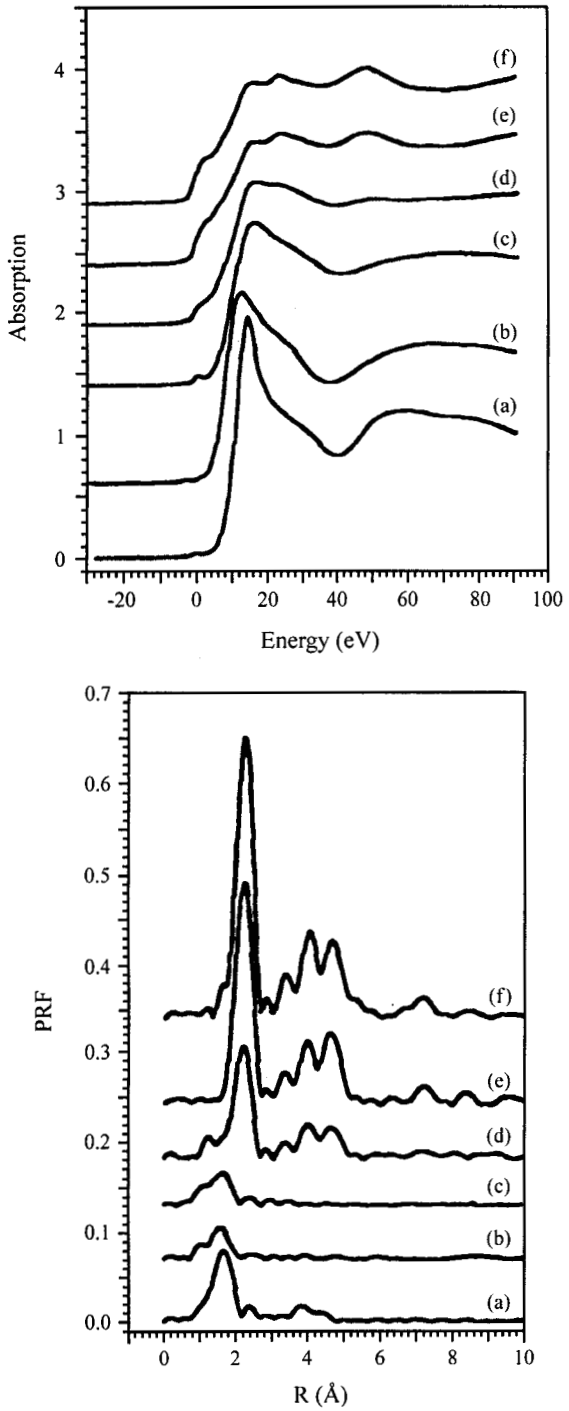

Figure 10. Co K edge XANES and corresponding PRF for the catalyst Pan+Co+Vulcan XC-72 as a function of temperature (a: pure Co acetate, Pan+Co+Vulcan XC-72 samples b: untreated, c: annealed at 800 °C, d: 900 °C, e: 1160 °C, f: Co metal).

Different attempts were made to reproduce the Ti K edge XANES and especially the pre-edge features, which clearly indicate that in addition to the dipole transition, quadrupole transitions have to be taken into account. Based on either the band structure approach[28,29] or MS[11], they were rather successful. On the other hand, a FEFF calculation[8] failed to reproduce the Ti K edge XANES, probably because not enough paths in the MS process were taken into account, whereas it reproduced very well the EXAFS oscillations (Fig. 12).

Fe/Ir multilayers: single scattering and polarization

Alternate Fe and Ir layers are deposited on an Ir buffer, which was grown on monocrystalline MgO. The specific magnetic properties of the superlattice grown in this way have led to structural studies by XAS using the polarization of the incident photon beam. In Fig. 13 the Fe K edge XANES are shown, taken in the perpendicular and parallel geometries for two samples with two different Fe thicknesses[30]. A comparison is made with the Fe K edge XANES

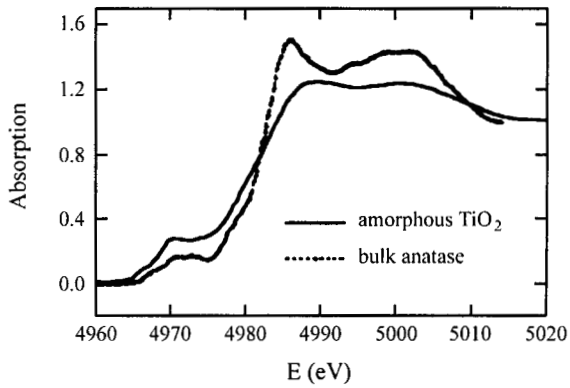

Figure 11. Ti K edge XANES for an electrochemically prepared amorphous TiO_2, as compared to crystalline anatase.

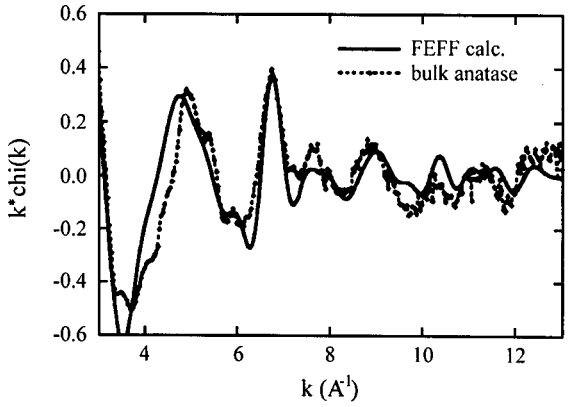

Figure 12. EXAFS oscillations at the Ti K edge in anatase: experimental and as calculated by FEFF.

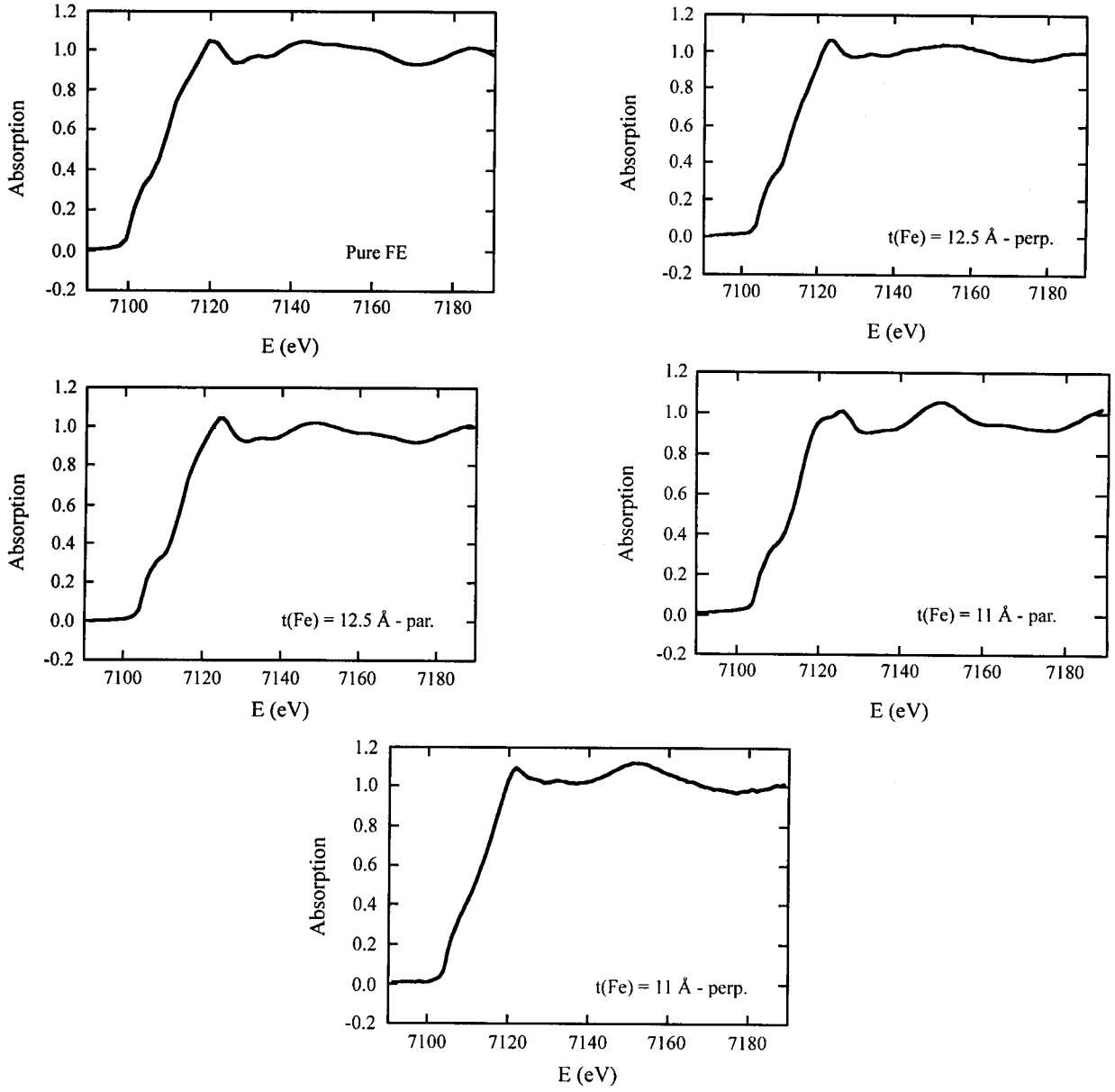

Figure 13. Fe K edge XANES for pure Fe and for Fe/Ir multilayers with t(Fe) = 12.5 Å and t(Fe) = 11 Å. For the superlattices, the spectra were measured in the parallel and perpendicular direction.

which corresponds to a bcc (body centered cubic) lattice. The XANES behavior changes, passing from a shape rather close to the one for pure Fe for the largest Fe thickness to a shape closer to the one for Cu (Fig. 9) for the thinnest Fe in the parallel direction.

A quantitative treatment of the EXAFS data revealed that the Fe layers are tetragonalized. The thinner the Fe layers, the larger the c/a ratio. The highest measured c/a is 1.22. An fcc (face centered cubic) lattice can be seen as a tetragonalized bcc one, called bct (body centered tetragonal), with a c/a ration of 1.414. Hence, this is the tetragonalization of the Fe lattice due to epitaxial growth on fcc Ir, which is responsible for the XANES modification. The question is why it is seen in the parallel direction and not in the perpendicular one. A FEFF calculation was performed where the experimentally measured lattice parameters were introduced. The anisotropy in the XANES shape, especially the split structure seen in the parallel geometry, instead of one peak in the perpendicular geometry, is very well reproduced. Moreover, a rather good agreement is seen over the whole k range between the experimental and calculated EXAFS spectra for both geometries. Analysis of all the contributions calculated by FEFF allowed us to determine which shell of atoms is responsible for the XANES anisotropy. This is the atom located at a distance of 4.60 Å from the absorber, with the following coordinates: 1.5 a, 0.5 a in the plane, and 0.5 c out of the plane. Since this atom is located out of the (100) plane, the backscattered wave experiences structural elongation with $c \neq a$. Its contribution to the backscattering process is high in the parallel direction (85.5%), while the same atom has a low contribution (17%) in the perpendicular direction. Hence, the induced splitting of the XANES shape is seen mainly in the parallel direction.

Another example where the FEFF program helped in the understanding of the epitaxial growth for Co on Cu(111) is given in Ref. 31.

Conclusion

Via these few examples, it is hoped that the reader has been convinced of the power of the XAS technique. From the technological point of view, sensitivity limits have been pushed back due to the development of very bright sources in new storage rings. This means that very diluted samples can be studied, or that very rapid processes can be followed and XAS can become a topological local probe.

The ease with which computer programs like FEFF[8], including single and multiple scattering processes, can be used, greatly help in the interpretation of both XANES and EXAFS spectra.

Acknowledgments

The author is very grateful to all his colleagues from LURE who through discussions and comments have helped him in writing this article. The author especially acknowledge G. Tourillon and A. Tadjeddine from LURE, C. Hague from the Laboratoire de Chimie Physique de Paris, and J. Mimault from the Laboratoire de Métallurgie Physique de Poitiers. I thank C. Vandamme for his help in preparing the figures.

References

1. Agarwal, B.K. *X-Ray Spectroscopy, An Introduction*, Springer Series in Optical Sciences 2. Springer Verlag, 1991, ed.; Vol. 15, chapter 7.
2. Fontaine, A. Les techniques de l'Ingénieur, December 1988, p 2698.
3. Lagarde, P. In *Initiation à la Spectroscopie d'Absorption des rayons X*, Eric Prouzet and Guy Ouvrard, Ed.; Nantes, 1994.
4. Michalowicz, A. *Logiciels pour la chimie*; Soc. Française de Chimie: Paris, 1991, 102; A. San Miguel, Physica B 208-209, 1995, 177; Bouldin, C.; Furenlid, L.; Elam, T. *Physica* 208-209, 1995, 190; Kuzmin, A. *Physica* 208-209, 1995, 175; 5 - McKale,A.G. *J.A.C.S.* **1988**, *110*, 3763.
5. McKale, A.G.; Veal, B.W.; Paulikas, A.P.; Chan, S.K.; Knapp., G.S.; *J. Am. Chem. Soc.* **1988**, *110*, 3763.
6. Teo, B.K.; Lee, P.A. *J. Am. Chem. Soc.* **1979**, 101:11, 2815.
7. Müller, J.E. In *EXAFS and Near Edge Structure III*; by K.O. Hodgson, B. Hedman, J.E. Penner-Hahn, Ed.; *Spinger Proc. Phys.* Springer; Berlin: Heidelberg, 1984; Vol. 2, p. 7.
8. Rehr, J.J.; Alberts, R.C. *Phys. Rev. B41* **1990**, 8139; Newville, M; Ravel, B.; Haskel, D.; Rehr, J.J.; Stern, E.A.; Yacoby, Y. *Physica* **1995**, *154*, 208-209.
9. Natoli, C.R.; Benfatto, M. In *EXAFS and Near Edge Structure IV* Lagarde, P.; Raoux, D.; Petiau, J. *J. Phys.* (Paris) Colloq., 1986, 47, C8-11.
10. Filipponi, A.; Di Cicco, A.; Tyson,T.A.; Natoli, C.R. *Solid State Comm.* **1991**, *78*, 265; Di Cicco, A. *Physica B* **1995**, *125*, 208-209.
11. Ruiz-López, M.F.; Muñoz-Paez, A. *J. Phys.: Condens. Matter 3* **1991**, 8981.
12. Behrens, Peter In *Trends in analytical chemistry*, Vol. 11, no. 7, 1992, p 237.
13. Fontaine, A.; Dartyge, E.; Jucha, A.; Tourillon, G. *Nucl. Instr. and Met.* **1987**, *A253*, 519.
14. Girardeau, T.; Mimault, J.; Jaouen, M.; Chartier, P. *Phys. Rev. B* **1992**, *46*, 7144.
15. Elam, W.T.; Kirkland, J.P.; Neiser, R.A.; Wolf, P.D. *Phys. Rev. B* **1988**; *38*, 26.

16. Mimault, J.; Faix, J.J.; Girardeau, T.; Jaouen, M.; Tourillon, G. *Meas. Sci. Technol.* **1994**, *5*, 482.
17. Goulon, J.; Goulon-Binet, C.; Cortes, R.; Dubois, J.M. *J. Physique* **1982**, *43*, 539.
18. Mariot, J.M.; Parent, P.; Traverse, A.; Lengauer, W.; Hague, C.F. *Nucl. Instr. and Met.* **1995**, *B97*, 123.
19. Marksteiner, P.; Weinberger, P.; Neckel, A.; Zeller, R.; Dederichs, P.H. *Phys. Rev.* **1986**, *B33*, 812.
20. Mariot, J.M.; Hague, C.F.; Lengauer, W.; Redinger, J.; Weinberger, P.; Beauprez, E. *Physica Scripta* **1990**, *41*, 584.
21. Traverse, A.; Parent, P.; Mimault, J.; Hagège, S.; Du, J. *Nucl. Instr. and Met.* **1994**, *B84*, 204.
22. Montano, P.A.; Shenoy, G.K.; Alp, E.E.; Schulze, W.; Urban, J. *Phys. Rev. Lett.* **1986**, *56*, 2076.
23. Messmer, R.P.; Knudson, S.K.; Jonhson, K.H.; Diamond, J.B.; Yang, C.Y. *Phys. Rev.* **1976**, *B13*, 1396.
24. Alves, M.C.M.; Dodelet, J.P.; Guay, D.; Ladouceur, M.; Tourillon, G. *J. Phys. Chem.* **1992**, *96*, 10898.
25. Scherson, D.A.; Gupta, S.L.; Fierro, C.; Yeager, E.B. *Electrochim. Acta* **1983**, *28*, 1205.
26. da Fonseca, C.; Traverse, A.; Tadjeddine, A.; Belo, M.C. *Jou. of Electroanalytical Chemistry* **1995**, 388 115.
27. Blondeau, G.; Froelicher, M.; Froment, M.; Hugot-Le Goff, A.; Brieu, M.; Calsouand F. Larroque, R. *J. Micros. Spectrosc. Electron.* **1977**, *2*, 27.
28. Poumellec, B.; Durham, P.J.; Guo, G.Y. *J. Phys.: Condens. Matter 3* **1991**, 8195.
29. Uozumi, T.; Okada, K.; Kotani, A.; Durmayer, O.; Kappler, J.P.; Beaurepaire, E.; Parlebas, J.C. *Europhys. Lett.* **1992**, *18*, 85.
30. Traverse, A.; Pizzini, S.; Andrieu, S.; Fontaine, A.; Piécuch, M. *Surf. Sci.* **1994**, *319*, 131.
31. Le Fevre, P.; Magnan, H.; Eckman, O.; Briois, V.; Chandesris, D., submitted for published in *Phys. Rev. B.*